Catalysis Today 147 (2009) 107–114

Contents lists available at ScienceDirect

Catalysis Today

journal homepage: www.elsevier.com/locate/cattod

Ethanol oxidation on metal oxide-supported platinum catalysts

L.M. Petkovic *, Sergey N. Rashkeev, D.M. Ginosar

Idaho National Laboratory, Idaho Falls, 2351 No. Boulevard, ID, 83415-2208, United States

ARTICLE INFO

Article history:
Available online 24 March 2009

Keywords:
Ethanol combustion
Ethanol oxidation
DFT
DRIFTS

ABSTRACT

Ethanol is a renewable fuel that can be used as an additive to gasoline (or its substitute) with the advantage of octane enhancement and reduced carbon monoxide exhaust emissions. However, on the standard three-way catalysts, the conversion of unburned ethanol is low because both ethanol and some of its partially oxidized derivatives are highly resistant to oxidation. A combination of first-principles density-functional theory (DFT)-based calculations and in situ diffuse reflectance infrared spectroscopy (DRIFTS) analysis was applied to uncover some of the fundamental phenomena associated with ethanol oxidation on Pt-containing catalysts. In particular, the objective was to analyze the role of the oxide (i.e., γ-Al_2O_3 or SiO_2) substrate on the ethanol oxidation activity. The results suggest that Pt nanoparticles trap and accumulate oxygen at their surface and perimeter sites and play the role of sites that burn ethanol molecules and their partially oxidized derivatives to the final products. The γ-Al_2O_3 surfaces provided higher mobility of the fragments of ethanol molecules than the SiO_2 surface and hence increased the supply rate of these species to the Pt particles. This in turn produces a higher conversion rate of unburned ethanol.

1. Introduction

The energy legislation signed into law in 2005 [1] established the use of higher volumes of renewable fuels such as ethanol and biodiesel. Beside energy security, one of the driving forces for using renewable fuels is the theoretically neutral greenhouse gas production when compared to gasoline. With respect to ethanol, it can be used as an additive or substitute for gasoline with the advantage of octane enhancement and reduced carbon monoxide (CO) exhaust emissions [2]. However, the combustion of alcohols poses new challenges particularly with regards to the increased formation of carbonyls such as aldehydes and ketones, which are irritants and also toxic air contaminants and important precursors to smog formation [3–9]. Research work performed in the 1980s indicated that Pt-containing catalysts were among the most promising materials for ethanol complete oxidation [10–12]. On standard three-way catalysts, the conversion of unburned ethanol is low [5] because both ethanol and acetaldehyde (i.e., product of partial oxidation of ethanol) are highly resistant to oxidation [13]. With respect to acetaldehyde in particular, experimental results showed that catalyst efficiency was worse for E3 (gasoline with 3%, v/v ethanol) than for E10 (gasoline with 10%, v/v ethanol) fuels [13]. Poulopoulos et al. [14] studied the effect of temperature and oxygen concentration on the catalytic destruction of 0.5% (volume/volume) ethanol in nitrogen over a typical three-way catalyst (Pt/Rh/Ce) and found the puzzling result that more acetaldehyde was produced under oxygen-deficit conditions than in the absence of oxygen. The reasons for these effects are currently unknown. Furthermore, there are reports that indicate that even methane emissions at tailpipe exhaust (in other words, downstream of the catalytic converter) are sometimes higher than at engine-out exhaust (upstream the catalytic converter) for ethanol-containing fuels [13].

The work reported here is an attempt to understand how the choice of the oxide substrate affects the rate of the ethanol oxidation on Pt/oxide catalysts by first-principles density-functional theory (DFT) calculations and in situ diffuse reflectance infrared spectroscopy (DRIFTS) analyses.

2. Experimental

Catalyst samples were prepared by the incipient wetness technique. Oxide supports, i.e., aluminum oxide (γ-Al_2O_3, 220 m^2/g) and silicon oxide (SiO_2, 250 m^2/g), and dihydrogen hexachloroplatinate (IV) hexahydrate ($H_2PtCl_6{\cdot}6H_2O$, 99.9%) were purchased from Alfa Aesar. The amount of noble metal added per gram of dry support was 0.05 millimoles. After impregnation, the samples were dried overnight at 378 K and calcined at 773 K for 2 h.

DRIFTS studies were performed on a Magna 750 FTIR system (Nicolet) equipped with a commercial high temperature DRIFTS cell (SpectraTech). Four hundred scans at 4 cm^{-1} resolution were collected using a KBr spectrum as the background. The samples

* Corresponding author. Tel.: +1 208 526 5033.
E-mail address: Lucia.Petkovic@inl.gov (L.M. Petkovic).

0920-5861/$ – see front matter © 2009 Elsevier B.V. All rights reserved.
doi:10.1016/j.cattod.2009.02.015

were finely ground and placed into the DRIFTS cell where they were re-calcined at 773 K for 30 min under 50 cm^3/min of flowing air (zero grade, MG Industries). Then, the samples were reduced at 573 K for 45 min under a flowing mixture of 10 cm^3/min of hydrogen (UHP, U.S. Welding) and 50 cm^3/min of nitrogen (UHP, U.S. Welding). Next, and before introducing ethanol to the cell, a series of six background spectra was collected between 303 and 773 K under a stream of 10 cm^3/min air and 50 cm^3/min nitrogen. These spectra were assumed to show the catalyst sample at each temperature before the introduction of ethanol. Subsequently, the temperature was stabilized at 303 K under the same mixture of air and nitrogen and an 80 μL pulse of liquid ethanol (HPLC/spectrophotometric grade, 200 proof, Sigma–Aldrich) was injected upstream of the cell to saturate the sample. Blank experiments indicated that a purging time of 60 min at 303 K was enough to remove all the ethanol weakly adsorbed in the system. Sixty minutes after the injection of ethanol a new series of spectra was collected at the same temperatures as the background spectra. The spectra reported were obtained by subtracting the spectra before the introduction of ethanol from the spectra after the introduction of ethanol.

Platinum oxidation state was analyzed by DRIFTS using CO (Matheson purity, 99.99%, Matheson Tri Gas) as the probe molecule. At the end of the DRIFTS experiment where ethanol was used, the cell was purged with nitrogen for 60 min at 773 K. Then, the temperature was decreased to room temperature under flowing nitrogen and the samples were exposed to flowing CO for 1 min. The cell was flushed with nitrogen for 60 min and the DRIFTS spectrum was collected. Freshly reduced samples and samples treated under flowing diluted air/nitrogen mixture without adsorption of ethanol were also analyzed by CO chemisorption. All DRIFTS spectra are reported in the Kubelka-Munk format and shown off-set for clarity.

3. Modeling

In order to investigate the role of different oxide surface and nanoparticle features in the ethanol oxidation, we constructed a large ensemble of metal nanoparticles of different size and shape on SiO_2 and γ-Al_2O_3 substrates and optimized their geometries using density-functional theory. Calculations were performed on a four-layer-thick SiO_2 (0 0 1) quartz slab, the oxygen-saturated quartz surface was fully hydrogenated. The density of free surface SiOH bonds at (0 0 1) quartz surface is determined to be 6.8/nm^2 in reasonable agreement with the experimental value of 6.3/nm^2 for fumed silica [15]. A five-atomic-layer-thick γ-Al_2O_3 slab was cut from the fully relaxed bulk structures [16] to expose the (110C) surface which is energetically preferred [17]. Large, periodically repeated supercells were used (15.4 Å × 13.8 Å × 23.5 Å for quartz, and 15.0 Å × 10.5 Å × 20.0 Å for γ-alumina). The vacuum layer between slabs was >12 Å. The adsorbates (nanoparticles, individual atoms, and molecules) and the top surface layers were fully relaxed (until quantum-mechanical forces acting on those atoms were smaller than 0.02 eV/Å), while the bottom layer was kept fixed.

The relaxed structures of the oxide surfaces were used for accommodation of individual Pt atoms or small Pt nanoparticles. Platinum nanoparticles containing between 5 and 35 atoms on top of the oxides were constructed as described previously [18] (by repeatedly adding single Pt atoms to existing structures and allowing them to relax again). For simulation of processes on larger nanoparticles, quasi-one-dimensional periodic rod-like structures containing a well-defined boundary between the nanoparticle and the substrate were also used. We did not perform a systematic search for the lowest-energy structures because: (i) the experimental formation of nanoparticles is not necessarily an equilibrium process and metastable configurations are likely to form; (ii) one can never ensure that the truly lowest-energy structure is found; (iii) an ensemble of nanoparticles with diverse local bonding and coordination numbers always provides a wide opportunity for exploring the most favorable conditions for their stability and activity.

Although the particles constructed in such a way cannot be taken to exactly replicate the size of metal nanoparticles used in real catalytic processes (some of these particles may contain thousands of atoms, and the first-principles calculations for such large systems are not affordable at the present), they offer the possibility to model the structure and electronic properties of the most catalytically active sites of the particles. Typically, these sites are closely related to the structural defects at the surface of the particle (edges, vertices, etc.), and are presented by low-coordinated atoms. This fact gives us a possibility to relate calculations for small particles to experiments performed on larger particles that still contain the same types of the defect sites.

The calculations were based on the generalized gradient approximation (GGA) for exchange and correlation, and plane waves [19]. We used the GGA of Perdew, Burke, and Ernzerhof (PBE) [20], which gives good results for chemisorption of molecules at transition-metal and oxide surfaces. Ultrasoft scalar relativistic pseudopotentials and the VASP codes [21,22] were used. The energy cutoff for the plane-wave basis was set at 400 eV, and all integrations over the Brillouin zone were done using the Monkhorst–Pack scheme with one k point in the relevant irreducible wedge [23]. Inclusion of additional k points was found to have minimal effect on the total-energy differences of interest here. The total number of atoms varied between 180 and 320 atoms for different periodic supercells. All the performed calculations were spin-polarized because Pt clusters exhibit magnetic ordering which in many cases significantly affects the reactions energies and activation barriers. Activation barriers were calculated using the nudged elastic band method [24].

4. Results

4.1. DRIFTS analyses

Difference spectra after adsorption of ethanol and desorption at increasing temperatures under flowing diluted air are shown in Figs. 1–4 for the samples γ-Al_2O_3, Pt/γ-Al_2O_3, SiO_2, and Pt/SiO_2. The analysis of those spectra was done by comparison of their infrared absorption peaks with the literature assignments summarized in Table 1. In particular, Fig. 1 shows the spectra of ethanol adsorbed on γ-Al_2O_3. C–H stretching (3000–2700 cm^{-1}) and bending (1500–1350 cm^{-1}) vibrations both corresponding to saturated aliphatic groups [25] are present. In more detail, these vibrations are assigned to methyl C–H asym./sym. stretch (2970/2897 cm^{-1}), methylene C–H asym./sym. stretch (2931/2868 cm^{-1}), and C–H bends (1490, 1451, 1448, and 1389 cm^{-1}). In particular, 1490 cm^{-1} may be assigned to methylene C–H bend and 1389 cm^{-1} to methyl C–H sym. bend. The band seen at 2727 cm^{-1} may be assigned to either or both "softened" C–H stretch produced by interaction of the ethanol alkyl groups with the surface [26,27] and α-C–H stretch of ethoxide species [28]. Monodentate, bidentate, and tridentate alkoxy groups have been proposed [10,27,29–31] upon adsorption of alcohols on oxide substrates. However, confirmation of adsorption as aluminum ethoxide by appearance of bands below 1200 cm^{-1} [32] was not possible. The strong vibration of the alumina framework combined to the relatively low intensity of the radiation reaching the detector when using the dome-cell DRIFTS setup produced a relatively low signal-to-noise ratio around the 1200 cm^{-1} region.

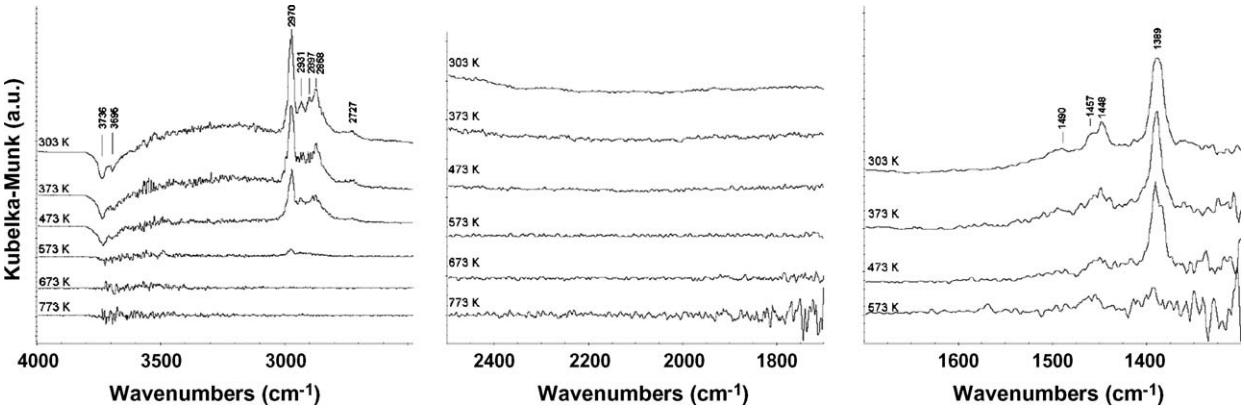

Fig. 1. DRIFTS spectra of ethanol adsorbed on γ-Al_2O_3 at 303 K and submitted to increasing temperatures under flowing diluted air.

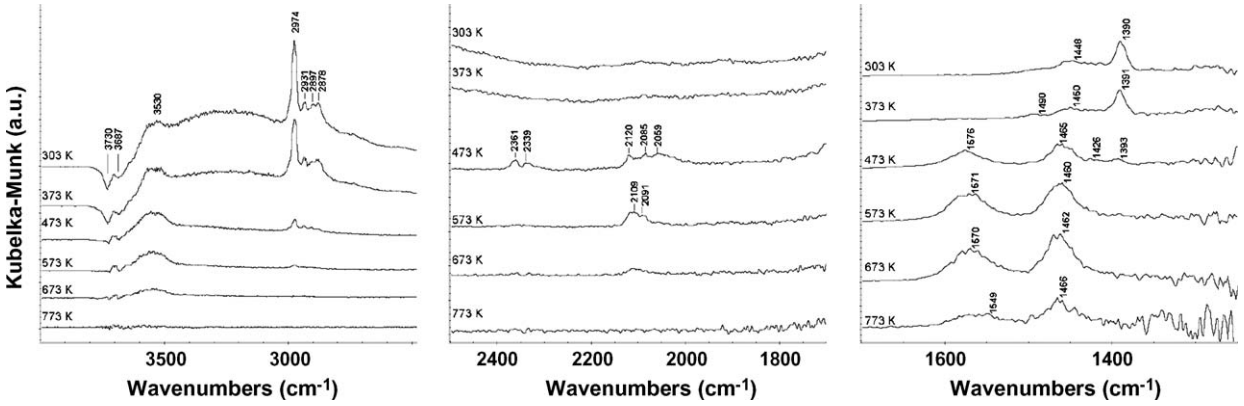

Fig. 2. DRIFTS spectra of ethanol adsorbed on Pt/γ-Al_2O_3 at 303 K and submitted to increasing temperatures under flowing diluted air.

The negative bands ca. 3700 cm^{-1} and the positive broad band within the 3600–3000 cm^{-1} range indicated hydrogen bonding between the alumina OH groups and the adsorbed ethanol. The monotonic decrease of the infrared bands as the temperature increased indicated that ethanol simply desorbed from the surface without oxidation or any other major reaction that could be detected by infrared spectroscopy. At 773 K the DRIFTS spectra did not show any major species remaining on the catalyst surface.

Fig. 2 shows the DRIFTS spectra for the case of adsorption of ethanol on Pt/γ-Al_2O_3. The spectrum obtained at 303 K showed infrared bands relatively similar to the ones shown by the Pt-free sample. Again, these bands indicate adsorption as hydrogen bonded molecules or ethoxide species on the catalyst surface. As the temperature was increased to 373 K, the decrease of the C–H stretch and bend vibrations indicated that part of the ethanol desorbed. At 473 K ethanol reaction was evidenced by the appearance of new bands. Carbon dioxide formation was apparent from the presence of the two bands at 2361 and 2339 cm^{-1} [36], which are assigned to gaseous or physisorbed CO_2. The bands at 2120, 2085, and 2059 cm^{-1} are assigned to carbon monoxide

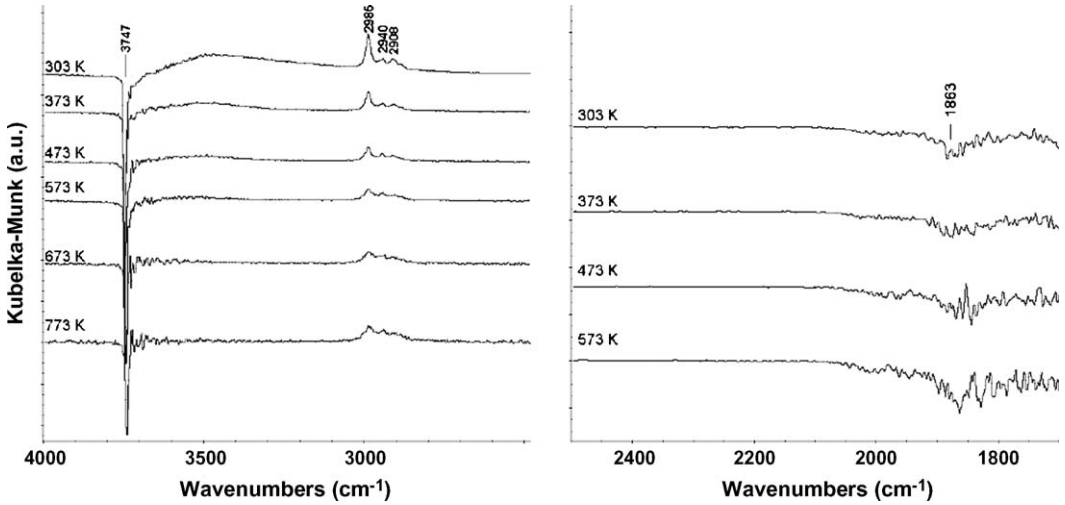

Fig. 3. DRIFTS spectra of ethanol adsorbed on SiO_2 at 303 K and submitted to increasing temperatures under flowing diluted air.

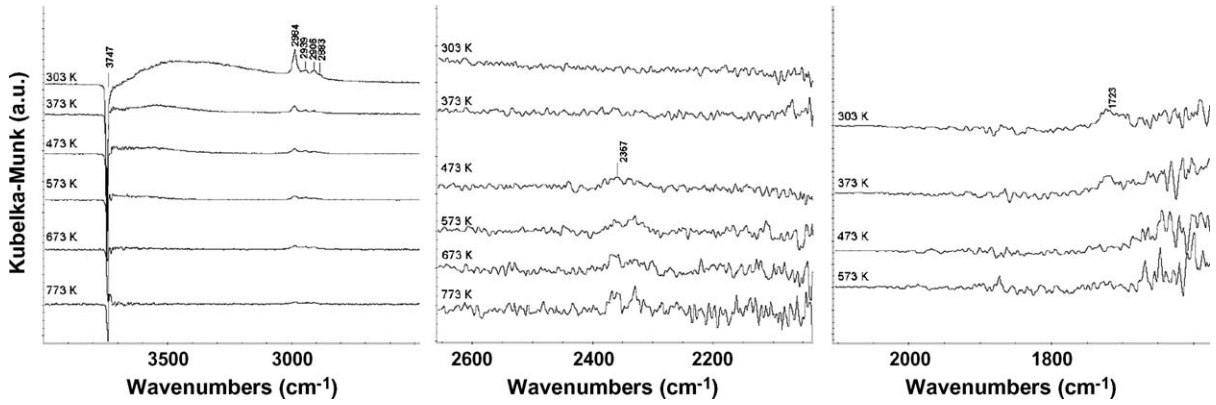

Fig. 4. DRIFTS spectra of ethanol adsorbed on Pt/SiO_2 at 303 K t 303 K and submitted to increasing temperatures under flowing diluted air.

Table 1
Literature assignments of vibration frequencies.

Assignment	Frequency (cm^{-1})	Source
Functional groups and alcohols adsorbed on oxides substrates		
Saturated methyl C–H asym./sym. stretch	2970–2950/2880–2860	[25]
Saturated methylene C–H asym./sym. stretch	2935–2915/2865–2845	[25]
Saturated methyl C–H asym./sym. bend	1470–1430/1380–1370	[25]
Saturated methylene C–H bend	1485–1445	[25]
"Softened" C–H stretch	ca. 2700	[26,27]
Ethoxide bands	1200–800	[32]
α-C–H asym. stretch of ethoxide	2700	[28]
COO acetate stretch asym./sym.	1550/1442	[33,34]
C–O stretch	1200–1050	[25]
C–O stretch of monodentate methoxy	1127	[32]
C–O stretch of bidentate methoxy	1060	[32]
Carbonyl CO stretch of surface acetate	1722	[10]
Carbon dioxide and carbonates		
Free carbonate (asym. stretch)	1415–1470	[35]
Monodentate carbonate (asym. stretch)	1420–1540	[35]
Monodentate carbonate (sym. stretch)	1330–1390	[35]
Gaseous carbon dioxide (asym. vibration)	Bands centered around 2350	[36]
Carbon monoxide		
Gaseous carbon monoxide	2143.2	[37]
CO linearly adsorbed on Pt	2110–2065	[38,39]
CO bridge adsorbed on Pt	1879–1694	[39]
CO on terrace Pt sites in presence of atomic O	2130	[38]
CO on PtO	2123	[40]
CO adsorbed on Pt–O sites	2120	[41]
CO adsorbed on Pt^{4+}	2186	[42]
CO adsorbed on Pt^{2+}	2138	[42]
Hydroxyl groups on silica and alumina surfaces		
Alumina O–H group stretch	3786, 3739, 3679	[43]
Silica O–H group stretch	3747	[43]
Si–O combination bands	1875	[44]

chemisorbed on platinum sites. When compared to gaseous carbon monoxide, which adsorbs infrared radiation around 2143 cm^{-1}[37] the carbon monoxide bands seen at 473 K indicate CO chemisorbed under a variety of coordination modes and/or on a number of Pt sites with different oxidation states or morphologies. The spectra at 473 K and higher temperatures are also showing bands at 1576 and 1465 cm^{-1}. The assignment of these bands is more challenging. Literature reports [33,34] have assigned frequencies of 1550/1442 cm^{-1} to asymmetric/symmetric COO acetate stretch of ethanol adsorbed on catalyst surfaces. In addition, stretching frequencies of chemisorbed CO_2 have been reported at 1330–1390 cm^{-1} (sym. stretch, monodentate), 1420–1540 cm^{-1} (asym. stretch, monodentate), and 1415–1470 cm^{-1} (asym. stretch-free carbonate) [35]. Then, the evolution of the bands seen on Fig. 2 suggests that the bands may be assigned to acetate or chemisorbed CO_2 at temperatures of 473 and 573 K and more likely to the latter at the higher temperatures of 673 and 773 K because of the absence of C–H stretching that would be expected in the case of acetates species. As the temperature was increased from 473 to 773 K the signals of chemisorbed CO and gaseous CO_2 decreased and at 773 K the spectrum showed only chemisorbed CO_2 or carbonate-like species.

Fig. 3 shows the difference spectra after adsorption of ethanol on SiO_2 at 303 K and desorption at increasing temperatures under flowing diluted air. C–H stretching (3000–2800 cm^{-1}) vibrations corresponding to saturated aliphatic groups [25] are clearly seen. Bending vibrations within the 1500–1350 cm^{-1} were not clearly seen (not shown) because of the strong silica vibrations in that range. The negative band at 3747 cm^{-1} [43] indicated disappearance of the OH groups initially present on the silica surface once ethanol was adsorbed. The negative peak at 1863 cm^{-1} is assigned here to interaction between adsorbed ethanol and Si–O bonds.

Note that Si–O combination bands absorb infrared absorption near 1863 cm^{-1} (i.e., 1875 cm^{-1} [44]). C–O stretching at ca. 1100 cm^{-1} was not seen.

Formation of ethanol oxidation products was not detected in any of the spectra. The decrease of the C–H stretching bands as the temperature increased indicated desorption. At 773 K there was still ethanol remaining on the surface in contrast with the γ-Al_2O_3 case which presented a relatively clean surface at that temperature. The DRIFTS spectra above 573 K show C–H stretch, not fully recovered Si–OH groups and lack of bridging H. These features may indicate the presence on the silica surface of ethanol fragments such as CH_3CH_2– that are difficult to desorb.

Fig. 4 shows the DRIFTS spectra of ethanol on Pt/SiO_2. As in the case of Pt-free SiO_2 the spectra show the expected C–H stretch and interaction of ethanol with Si–OH groups. However, in the case of Pt/SiO_2 the spectra also presented a band at 1723 cm^{-1} at 303 and 373 K. This band was absent on the spectrum of SiO_2. Gonzalez and Nagai [10] assigned a band at 1722 cm^{-1} observed when ethanol was oxidized on a Pt/SiO_2 catalyst to the carbonyl stretching frequency of a surface acetate species. At 473 K and higher temperatures some CO_2 formation (2357 cm^{-1}) was detected just above the noise level. Carbon monoxide infrared bands above the detection limits were not seen.

Fig. 5 shows the DRIFTS spectra after chemisorption of carbon monoxide on (a) a freshly reduced Pt/Al_2O_3 catalyst sample, (b) a Pt/Al_2O_3 sample submitted to the same conditions as the experiment but without introducing ethanol, (c) the spent Pt/Al_2O_3 sample at the end of the experiment shown in Fig. 2, and the spent Pt/SiO_2 sample at the end of the experiment shown in Fig. 4. The fresh reduced sample (a) showed a peak at 2070 cm^{-1} along with a shoulder at 2119 cm^{-1}. A smaller peak at 1840 cm^{-1} is also seen. Both (b) and (c) samples showed only a peak at 2119 cm^{-1}. Previous reports have assigned frequencies in the 2110–2065 cm^{-1} region to CO linearly coordinated to Pt^0 sites, on the 1879–1694 cm^{-1} region to multibonded, bridged, and threefold bonded CO species [38,39], and on the 2186–2120 cm^{-1} to CO adsorbed on cationic or oxygen covered Pt sites [40–42,45]. Comparing these assignments with the spectra seen in Fig. 5, it can be concluded that the peak at 2070 cm^{-1} indicates Pt^0 sites and the shoulder and peaks at 2119 cm^{-1} indicate oxidized Pt sites. These findings indicate that the platinum particles dispersed on the γ-Al_2O_3 support were oxidized when contacted with the diluted air stream present in both the blank experiment and in the experiment where ethanol was introduced. In contrast, the state of Pt on SiO_2 was metallic (i.e., 2081 cm^{-1}).

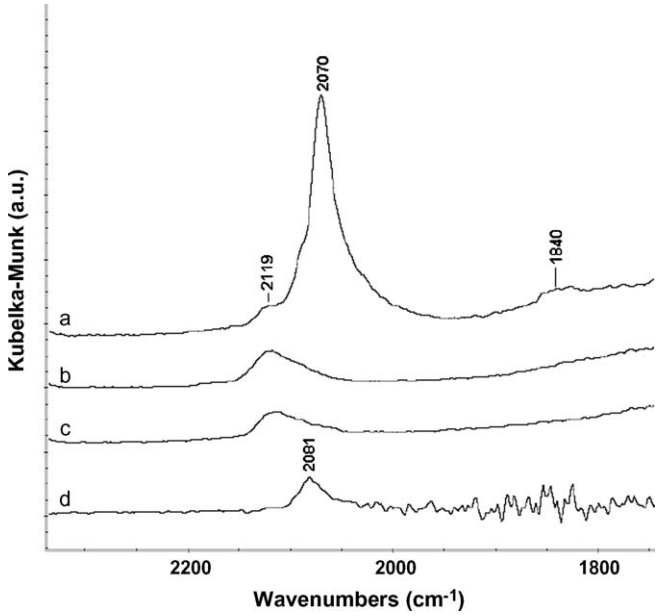

Fig. 5. DRIFTS spectra of CO adsorbed at 303 K on (a) fresh reduced Pt/γ-Al_2O_3, (b) blank experiment on Pt/γ-Al_2O_3 and no ethanol, (c) spent Pt/γ-Al_2O_3, and (d) spent Pt/SiO_2.

Summarizing the results obtained by DRIFTS it may be stated that Pt-free supports alone did not present any significant activity for oxidation of ethanol. The presence of the noble metal was necessary for the catalyst to show activity for the oxidation reaction. The intermediate products detected depended on the support: on Pt/SiO_2, acetate was detected at ca. room temperature and only a minor CO_2 infrared signal at higher temperatures. On Pt/Al_2O_3, CO and CO_2 were detected.

For both alumina samples, the alumina surface OH features were almost completely recovered after ethanol desorption/oxidation as the temperature was increased to 773 K. For the silica samples, higher temperatures were required to desorb the ethanol and its fragments and there were still C–H stretching features and decreased sylanol OH stretching remaining at the highest temperature studied. This indicated that the bonding between ethanol fragments, perhaps CH_3CH_2–, and the silica surface was stronger than on the surface of alumina. This was confirmed by DFT calculations as shown in the next section. The relatively lower activity of the Pt/SiO_2 catalyst may be related to both the stronger adsorption of ethanol and perhaps larger platinum particles. Under working conditions platinum particles on alumina were oxidized. In contrast only Pt metal was detected on the silica-supported catalyst.

4.2. First-principles calculations and modeling

Oxidation of ethanol and its partially oxidized derivatives may occur in three different ways: (a) both the O_2 and CH_3CH_2OH (ethanol) molecules react in the gas phase; (b) one of the reacting molecules is attached to the surface while another molecule comes to the reactive zone from the gas phase; (c) both of the reactants are attached to the surface and react there. Typically, mechanism (c) is statistically preferred, especially if the reacting molecules (or at least some of them) exhibit high mobility at the surface which increases the molecular collision rate.

Let us compare fully hydrogenated SiO_2 (0 0 1) quartz and γ-Al_2O_3 (110C) surfaces. All the O–H bonds at the hydrogenated oxygen-saturated quartz surface are equivalent and have the same bond energy (~4.5 eV). At the γ-Al_2O_3 surface, the O–H binding energy depends on the coordination of O atom and may vary in a wide range between 1.2 and 3.0 eV [18]. The presence of one OH peak on silica (3747 cm^{-1}) and several OHs (3730, 3687 cm^{-1}) on alumina is confirmed by the spectra shown in Figs. 1–4. Thus, hydrogen can be removed from the alumina surface much easier than from silica. In particular, H atoms can be removed by the oxygen component of the air flow near the surface (the same flow that is employed for the ethanol oxidation). It is easy to check that the reaction, $4H^{(ad)} + O_2{}^{(g)} = 2H_2O^{(g)}$, where the superscript "g" means the gas phase, and "ad" related to adsorbed atom, is highly endothermic (~4 eV) and likely never occurs for hydrogen adsorbed at the silica surface, and highly exothermic (~2.0–9.2 eV) at the alumina surface (likely to occur). Another mechanism for H disappearing from the alumina surface is its migration into the bulk of the oxide—in particular, this process is important for a breakdown of the oxide film on top of the Al metal and an initiation of the corrosion at the metal surface [18]. Therefore, the initially hydrogenated SiO_2 surface will remain fully hydrogenated while the alumina surface will always have a tendency to loose some hydrogen and exhibit some "bare" oxygen atoms.

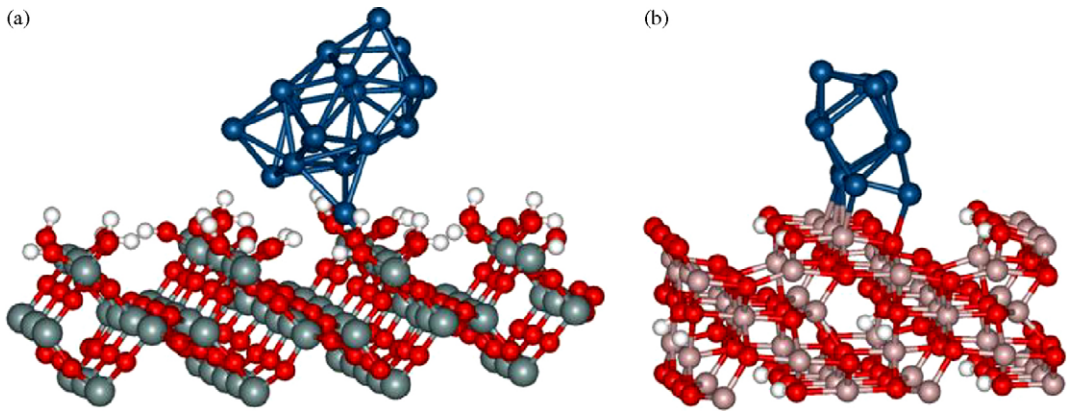

Fig. 6. Eighteen atoms Pt nanoparticle positioned on top of fully hydrogenated SiO_2 (0 0 1) quartz surface (a), and 12-atoms Pt nanoparticle positioned on the γ-Al_2O_3 (110C) surface (b). Si atoms are shown in grey, Al in light brown, O in red, H in white, Pt in blue. (For interpretation of the references to color in this figure legend, the reader is referred to the web version of the article.)

The difference in the hydrogenation behavior causes the difference in the shape of Pt nanoparticles attached to the silica and alumina surfaces. Fig. 6 shows examples of two small (with the diameters between 0.5 and 1.0 nm) Pt clusters positioned on top of these two surfaces. One cannot expect to find many dehydrogenated sites at the SiO_2 surface. Therefore, the growth of the nanoparticle starts around a single dehydrogenated site at the surface (in this case, around a dangling oxygen at the surface). This nanoparticle forms in the shape of a mushroom that is anchored to the surface with a single Pt atom. Such a particle does not have any perimeter sites, and all the catalytic processes occur at surface sites in a way similar to an unsupported metal particle.

If there are other neighboring dehydrogenated sites at the silica surface, the Pt nanoparticle may be anchored with more than one atom. However, these sites should exist before the deposition of Pt atoms at the surface, i.e., the nanoparticle does not bind to any other atoms at the surface except these pre-existing dehydrogenated sites. At the alumina surface there are many dehydrogenated sites, and the nanoparticle could be attached to many surface oxygen atoms. We found, however, that Pt atoms form stronger bonds with Al (not O) atoms at the surface. This is another argument in favor of the scenario that surface hydrogen (attached to oxygen) and dehydrogenated sites play only a minor role in Pt clustering at the γ-alumina surface. Pt nanoparticles at alumina surfaces have perimeter sites that may be also involved in the catalytic processes (in addition to the nanoparticles surface atoms). A similar behavior of catalytic Ag clusters at the alumina surface was also mentioned in Ref. [46]. However, our main conclusion (see below) is that the differences in shape, anchoring mechanism, and perimeter sites of Pt nanoparticles at the two different oxide surface play just a minor role in the ethanol oxidation processes which is mainly defined by interactions between ethanol molecules and the oxide surfaces.

An CH_3CH_2OH molecule arriving at the surface can attach to both the oxide or one of the Pt particles anchored at the oxide. The most likely scenario for interaction between an ethanol molecule and the oxide surface is the formation of hydrogen bonds between the two OH groups (one is positioned at the molecule, another—at the surface), with a subsequent formation of a water molecule that leaves the surface, and an attachment of the CH_3CH_2– fragment to an oxygen atom at the surface. A simple estimate shows that such a reaction is not exothermic or endothermic ($\Delta E \sim 0$) for both oxides because the initial and final numbers of the O–H and C–O bonds are the same. Nudged elastic band calculations also give rather a low barrier for such a reaction (~0.5–1.0 eV depending on the initial configuration and the site at the oxide surface), i.e., such an attachment of the CH_3CH_2– fragment to the oxide is very likely. It is worth mentioning that there are two alternatives that may be envisioned for the formation of alkoxy groups on oxide substrates: the oxygen atom of the chemisorbed alkoxy group being provided by (i) the adsorbate or (ii) the oxide surface. Literature reports show experimental evidence pointing to both cases [32,47]. For our modeling calculations we have considered the oxygen of the alkoxy group as occupying the place of the substrate surface oxygen. For the alumina case, the substrate surface oxygen is three-cordinated; for the silica case, it is two-coordinated.

Oxidation, conversion, and dehydrogenation of ethanol and methanol at different metal and metal alloy catalysts (including Pt) have been extensively studied experimentally and theoretically [46,48]. It is generally agreed that all of these reactions are multistep processes that involve a significant number of intermediate products that are adsorbed at the metal surface. These products include acetaldehyde, acetic acid, surface oxametallacycles, metallaoxetanes [49], and even enolic species [46]. The details of the conversion process depend on the chemical composition of the metal or metal alloy surface [49,50] as well as on the nature of the substrate [46,51,52]. In all of these considerations, however, the role of the oxide substrate was restricted to providing additional anchoring states near the perimeter sites of the metal particles that bind some atoms of intermediate adsorbates [46,52]. The complexity of mechanisms of the catalytic ethanol conversion are ruled by the whole set of different reaction barriers and transition states and a very delicate balance between the binding energies of different atomic species on different active sites at the surface of the catalyst. For example, it is well-known that platinum does not form hydrates because of the weakness of the Pt–H bond (according to experiment [53] it does not exceed 17–31 kcal/mol). This binding energy is much weaker than the C–H and O–H bonds in the CH_3CH_2OH molecule. However, dehydrogenation of ethanol still occurs due to the fact that the intermediate product (formed by the ethanol molecule after it lost some hydrogen atoms) attaches to the catalyst and forms Pt–C and Pt–O bonds that are also strong (actually, the bonding energy depends on many factors including the geometry and size of the Pt particle, the nature of the substrate, etc.).

In this work we are not going to analyze all of the numerous issues related to the CH_3CH_2OH conversion. Our main goal is to understand how the choice of the oxide substrate affects the rate of the ethanol oxidation on Pt/oxide catalysts. The presence of O_2 in the feed flow introduces some changes into the ethanol conversion. For example, reports indicated that O_2 favors the oxidation of acetyl species to acetate species and the formation of CO_2 (instead of CO) on Pt/CeO_2 catalysts [51]. The reason for such behavior is clear—Pt particle surfaces always have a tendency to capture

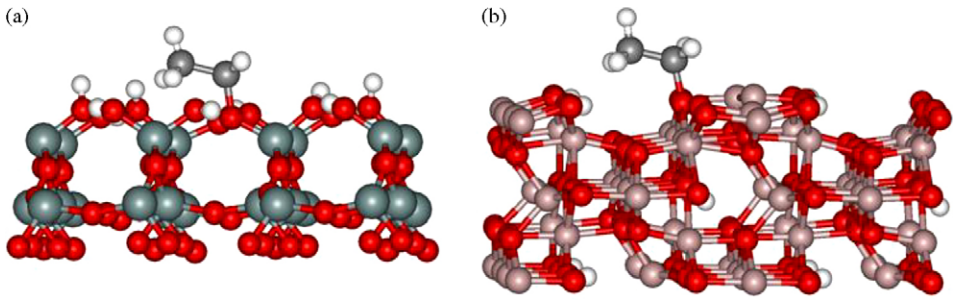

Fig. 7. A schematic of the CH_3CH_2– intermediates anchored at SiO_2 (001) quartz surface (a), and at the γ-Al_2O_3 (110C) surface (b). Si atoms are shown in large grey balls, C in small grey balls, Al in light brown, O in red, H in white. (For interpretation of the references to color in this figure legend, the reader is referred to the web version of the article.)

oxygen molecules and keep them or split them to atomic oxygen, consequently, adsorbed ethanol intermediates get a better chance to react with oxygen at the surface of the particle than with oxygen molecules from the feed flow gas (mechanism (c)—see the beginning of this section). The perimeters of these nanoparticles may also assist in the oxidation process as was shown in Refs. [46,52]. At a flat Pt (1 1 1) surface, the O_2 molecule binding energy is 1.8 eV, O atom—3.6 eV, the reaction barrier for splitting the O_2 molecule is 1.2 eV, the migration barrier for atomic oxygen at the surface—0.5 eV [54]. For a smaller nanoparticle, the atomic state of oxygen becomes more favourable—the splitting barrier for the O_2 molecule becomes lower, the binding energy of an O atom to the particle may increase up to 5.5 eV (for a 12 atoms particle). Therefore, the catalytic activity in very small Pt nanoparticles may decrease in comparison with the activity of bigger particles [18]. The reason for such a behavior is that the Pt–O bond is very strong when the oxygen atom is attached to low-coordinated Pt atoms and it becomes energetically unfavorable to form new C–O, or H–O bonds and remove the reaction products away from the surface. This may explain the more oxidized state of the Pt at the end of the experiment using Pt/alumina when compared with the Pt/silica as shown in Fig. 5. For the alumina case, the stronger binding of the Pt particle to the support may lead to formation of less rounded particles. These platinum particles are likely to have higher number of low-coordination Pt atoms where oxygen atoms may chemisorb more strongly than on the surface Pt deposited on silica.

Now we can explain the differences between the Pt/SiO_2 and Pt/Al_2O_3 catalysts observed in the DRIFTS experiments described above. If the ethanol molecule attaches to one of the platinum nanoparticles positioned on silica or alumina, its conversion and oxidation is mainly related to the properties of this nanoparticle—its diameter and the number of low-coordinated (most active) sites at the particle. Most likely, the ethanol molecule will be completely converted (to simple products such as CO, CO_2, H_2O, hydrogen, methane, etc.) at this single particle. The perimeter of the particle (present for the case of Pt/alumina catalyst) may also assist in converting ethanol.

If, however, the ethanol molecule first adsorbs on or reacts with the oxide substrate and forms the CH_3CH_2– intermediate anchored at the oxide surface according to the mechanism described above (Fig. 7), its further conversion will develop in a different way. At SiO_2 surface, the calculated binding energy between the CH_3CH_2– intermediate and an O atom is about 4.2 eV. Moreover, the surrounding SiO_2 surface is fully hydrogenated, i.e., there are no "vacant" sites where the intermediate can adsorb. These two factors make any migration of the CH_3CH_2– practically impossible. Once attached to the surface, this group will stay at the place where it was initially attached and react only with molecules in the gas phase (the mechanism (b) described in the beginning of this section). The rate of conversion by this mechanism will be slow. At the alumina surface, the binding energy of the CH_3CH_2– intermediate to different O atoms does not exceed 0.7 eV (the differences in binding is related to different possible coordination of O atoms at alumina surface), and the migration energy (of jumps between different O atoms) does not exceed 0.5 eV. Such a large difference in the intermediate binding energy for silica and alumina is mainly related to the fact that the dangling oxygen atom at a silica surface is two coordinated and attached to one Si atom while each of the O atoms at an alumina surface is attached to at least two aluminum atoms and an Al atom reacts with O stronger than Si. Therefore, any surface O atom in alumina does not have enough electrons to form a strong covalent bond with the C atom of the CH_3CH_2– intermediate. This means that the CH_3CH_2– intermediate will migrate around the alumina surface before it reaches one of the Pt nanoparticles where it will be trapped, converted, and oxidized by oxygen anchored and accumulated at the surface of the nanoparticle. Ethanol on silica stayed for a longer time (i.e., required higher temperatures to desorb) than on alumina as seen by the DRIFTS analyses shown above.

To this point, we have studied the energetics of the ethanol fragment attached to the substrate surface and assumed that the oxygen formed on the platinum particle was not mobile. However, one may also think that oxygen mobility and spill over play a role in catalyst activity. Although not reported here, preliminary calculations, which will be the focus of a future paper, have shown that when atomic oxygen produced on the platinum surface spills over the alumina surface, the energetics are such that the atomic oxygen will likely be less mobile than the ethanol fragments. For the silica case, the barrier to spill over atomic oxygen is even much higher than for alumina.

Therefore, we conclude that first-principles DFT calculations agree well with the DRIFTS analysis. In a few words, DRIFTS showed that under oxidation conditions silica catalysts required higher temperatures than alumina catalysts to desorb ethanol and its fragments. DFT showed that, for CH_3CH_2– fragments, energies not exceeding 0.7 eV were involved in the attachment to the alumina surface and an energy of 4.2 eV for the case of silica. The combination of these methods provides a complete and consistent explanation of the role of the oxide (γ-Al_2O_3 or SiO_2) substrate and Pt nanoparticles in the ethanol oxidation activity process.

5. Conclusions

A combination of in situ DRIFTS analysis and first-principles DFT-based calculations were used to uncover some of the fundamental phenomena associated with ethanol oxidation on Pt-containing catalysts. Pt nanoparticles trap and accumulate oxygen at their surface and perimeter sites and play the role of sites that burn ethanol molecules and their partially oxidized derivatives to the "final" products. The oxide support plays a very important role in the catalytic activity for ethanol oxidation. It not only affects the size and shape of the noble metal nanoparticles but also affects the mobility of the ethanol molecule or its fragments adsorbed on the support. Oxide surfaces with higher mobility of

the fragments of ethanol molecules provide higher supply rate for these species to the Pt particles where they will be oxidized.

Acknowledgements

Work supported through the INL Laboratory-Directed Research and Development Program under DOE/NE Idaho Operations Office Contract DE-AC07-05ID14517.

References

[1] Energy Policy Act of 2005, available at http://www.ethanolrfa.org/objects/pdf/PublicPolicy/Regulations/EnergyConf.pdf on July 05, 2007.
[2] R. Magnusson, C. Nilsson, B. Andersson, Environ. Sci. Technol. 36 (2002) 1656.
[3] R.M. Bata, V.P. Roan, J. Eng. Gas Turb. Power-Trans. ASME 111 (1989) 432.
[4] P.J. Gabele, J. Air Waste Manage. Assoc. 45 (1995) 770.
[5] T. Burgi, R. Wirz, A. Baiker, J. Phys. Chem. B 107 (2003) 6774.
[6] K. Ito, K. Kurata, Bull. JSME-Jap. Soc. Mech. Eng. 28 (1985) 2028.
[7] R.P. McGinty, N.P. Dent, Environ. Technol. 16 (1995) 603.
[8] E. Zervas, X. Montagne, J. Lahaye, Environ. Sci. Technol. 36 (2002) 2414.
[9] D. Karman, Ethanol fuelled motor vehicle emissions: a literature review. Available at http://www.cleanairnet.org/caiasia/1412/articles-69504_paper.pdf on July 08, 2007, 2003, Submitted to Air Health Effects Division, Health Canada, May 2003.
[10] R.D. Gonzalez, M. Nagai, Appl. Catal. 18 (1985) 57.
[11] R.W. McCabe, P.J. Mitchell, Ind. Eng. Chem. Prod. Res. Dev. 23 (1984) 196.
[12] Y.F.Y. Yao, Ind. Eng. Chem. Proc. Des. Dev. 23 (1984) 60.
[13] S.G. Poulopoulos, D.P. Samaras, C. Philippopoulos, Atmos. Environ. 35 (2001) 4399.
[14] S.G. Poulopoulos, H.P. Grigoropoulou, C.J. Philippopoulos, Catal. Lett. 78 (2002) 291.
[15] C.H.C. Liu, G.E. Maciel, Anal. Chem. 68 (1996) 1401.
[16] K. Sohlberg, S.J. Pennycook, S.T. Pantelides, J. Am. Chem. Soc. 121 (1999) 7493.
[17] H. Knozinger, P. Ratnasamy, Catal. Rev. Sci. Eng. 17 (1978) 31.
[18] S.N. Rashkeev, A.R. Lupini, S.H. Overbury, S.J. Pennycook, S.T. Pantelides, Phys. Rev. B 76 (2007) 035438.
[19] M.C. Payne, M.P. Teter, D.C. Allan, T.A. Arias, J.D. Joannopoulos, Rev. Mod. Phys. 64 (1992) 1045.
[20] J.P. Perdew, K. Burke, M. Ernzerhof, Phys. Rev. Lett. 77 (1996) 3865.
[21] G. Kresse, J. Hafner, Phys. Rev. B 48 (1993) 13115.
[22] G. Kresse, J. Furthmuller, Phys. Rev. B 54 (1996) 11169.
[23] D.J. Chadi, M.L. Cohen, Phys. Rev. B 8 (1973) 5747.
[24] H. Johnson, G. Mills, K.W. Jacobsen, in: B.J. Berne, G. Cicotti, D.F. Coker (Eds.), Classical and Quantum Dynamics in Condensed Phase Systems, World Scientific, River Edge, NJ, 1998.
[25] J. Coates, Interpretation of Infrared Spectra, A practical Approach, John Wiley & Sons Ltd., Chichester, 2000.
[26] J.E. Demuth, H. Ibach, S. Lehwald, Phys. Rev. Lett. 40 (1978) 1044.
[27] S. Golay, R. Doepper, A. Renken, Appl. Catal. A 172 (1998) 97.
[28] S. Matsuta, T. Asada, K. Kitaura, J. Electrochem. Soc. 147 (2000) 1695.
[29] R.G. Greenler, J. Chem. Phys. 37 (1962) 2094.
[30] L.J. Burcham, L.E. Briand, I.E. Wachs, Langmuir 17 (2001) 6164.
[31] M. Domok, M. Toth, J. Rasko, A. Erdohelyi, Appl. Catal. B 69 (2007) 262.
[32] M. Bensitel, V. Moravek, J. Lamotte, O. Saur, J.C. Lavalley, Spectrochim. Acta Part A: Mol. Biol. 43 (1987) 1487.
[33] L. Gamble, L.S. Jung, C.T. Campbell, Surf. Sci. 348 (1996) 1.
[34] W. Rachmady, M.A. Vannice, J. Catal. 207 (2002) 317.
[35] A.M. Turek, I.E. Wachs, E. Decanio, J. Phys. Chem. 96 (1992) 5000.
[36] D. Williams, Methods of Experimental Physics, vol. 3, Academic Press, 1976.
[37] D.J. Yates, J. Phys. Chem. 65 (1961) 746.
[38] K. Tanaka, J.M. White, J. Catal. 79 (1983) 81.
[39] R. Barth, R. Pitchai, R.L. Anderson, X.E. Verykios, J. Catal. 116 (1989) 61.
[40] Y. Barshad, X. Zhou, E. Gulari, J. Catal. 94 (1985) 141.
[41] M. Primet, J. Catal. 88 (1984) 273.
[42] K.I. Hadjiivanov, J. Chem. Soc. Faraday Trans. 94 (1998) 1901.
[43] C.M. Koretsky, D.A. Sverjensky, J.W. Salisbury, D.M. Daria, Geochim. Cosmochim. Acta 61 (1997) 2193.
[44] H.A. Benesi, A.C. Jones, J. Phys. Chem. 63 (1959) 179.
[45] A.Y. Stakheev, E.S. Shpiro, O.P. Tkachenko, N.I. Jaeger, G. SchulzEkloff, J. Catal. 169 (1997) 382.
[46] Y.B. Yu, H.W. Gao, H. He, Catal. Today 93 (2004) 805.
[47] T.P. Beebe, J.E. Crowell, J.T. Yates, J. Phys. Chem. 92 (1988) 1296.
[48] J. Lichtenberger, D. Lee, E. Iglesia, Phys. Chem. Chem. Phys. 9 (2007) 4902.
[49] G.S. Jones, M. Mavrikakis, M.A. Barteau, J.M. Vohs, J. Am. Chem. Soc. 120 (1998) 3196.
[50] R. Alcala, J.W. Shabaker, G.W. Huber, M.A. Sanchez-Castillo, J.A. Dumesic, J. Phys. Chem. B 109 (2005) 2074.
[51] A.M. Silva, L.O.O. Costa, A. Barandas, L.E.P. Borges, L.V. Mattos, F.B. Noronha, Catal. Today 133–135 (2008) 755.
[52] H.L. Chen, S.H. Liu, J.J. Ho, J. Phys. Chem. B 110 (2006) 14816.
[53] W.H. Weinberg, R.P. Merrill, Surf. Sci. 33 (1972) 493.
[54] S.N. Rashkeev, D.M. Ginosar, L.M. Petkovic, H.H. Farrell, Catal. Today 130 (2009) 291.